J Neurophysiol 98: 2382–2398, 2007.
First published July 25, 2007; doi:10.1152/jn.00572.2007.

Parameter Space Analysis Suggests Multi-Site Plasticity Contributes to Motor Pattern Initiation in *Tritonia*

Robert J. Calin-Jageman,[1] Mark J. Tunstall,[5,✠] Brett D. Mensh,[2,3] Paul S. Katz,[1] and William N. Frost[4]
[1]*Department of Biology, Georgia State University, Atlanta, Georgia;* [2]*Department of Neuroscience, Columbia University College of Physicians and Surgeons, New York, New York;* [3]*Department of Physical Medicine and Rehabilitation, Harvard Medical School, Cambridge, Massachusetts;* [4]*Department of Cell Biology and Anatomy, The Chicago Medical School, Rosalind Franklin University of Medicine and Science; and* [5]*Department of Neurobiology and Anatomy, University of Texas Health Sciences Center, Houston, Texas*

Submitted 22 May 2007; accepted in final form 20 July 2007

Calin-Jageman RJ, Tunstall MJ, Mensh BD, Katz PS, Frost WN. Parameter space analysis suggests multi-site plasticity contributes to motor pattern initiation in *Tritonia*. *J Neurophysiol* 98: 2382–2398, 2007. First published July 25, 2007; doi:10.1152/jn.00572.2007. This research examines the mechanisms that initiate rhythmic activity in the episodic central pattern generator (CPG) underlying escape swimming in the gastropod mollusk *Tritonia diomedea.* Activation of the network is triggered by extrinsic excitatory input but also accompanied by intrinsic neuromodulation and the recruitment of additional excitation into the circuit. To examine how these factors influence circuit activation, a detailed simulation of the unmodulated CPG network was constructed from an extensive set of physiological measurements. In this model, extrinsic input alone is insufficient to initiate rhythmic activity, confirming that additional processes are involved in circuit activation. However, incorporating known neuromodulatory and polysynaptic effects into the model still failed to enable rhythmic activity, suggesting that additional circuit features are also required. To delineate the additional activation requirements, a large-scale parameter-space analysis was conducted ($\sim 2 \times 10^6$ configurations). The results suggest that initiation of the swim motor pattern requires substantial reconfiguration at multiple sites within the network, especially to recruit ventral swim interneuron-B (VSI) activity and increase coupling between the dorsal swim interneurons (DSIs) and cerebral neuron 2 (C2) coupling. Within the parameter space examined, we observed a tendency for rhythmic activity to be spontaneous and self-sustaining. This suggests that initiation of episodic rhythmic activity may involve temporarily restructuring a nonrhythmic network into a persistent oscillator. In particular, the time course of neuromodulatory effects may control both activation and termination of rhythmic bursting.

INTRODUCTION

Many intermittent rhythmic behaviors are mediated by episodic central pattern generators (CPGs), indicating that the initiation, maintenance, and termination of rhythmic activity represent important regulatory tasks for the nervous system (Eisenhart et al. 2000; Fredman and Jahan-Parwar 1980; Jing and Gillette 1995; Rosen et al. 1991). Episodic CPGs are often controlled by extrinsic inputs (Lennard et al. 1980), such as the mesencephalic locomotor region, which can initiate locomotion in mammals (Jordan 1998; Shik et al. 1966). Most of these CPGs have additional activation requirements, including activation of neuromodulatory elements (Nagy et al. 1994; Nusbaum and Kristan 1986) and/or alteration of the CPG's cellular and synaptic properties (Dale and Gilday 1996; Staras et al. 2003). It is still unclear, however, how multiple conditions interact to gate the activation of rhythmic network activity. Here we examine this issue in the episodic CPG underlying escape swimming in the gastropod mollusk, *Tritonia diomedea.*

The *Tritonia* escape swim is triggered by contact with a predatory sea star and consists of a ~1-min series of alternating dorsal/ventral body flexions (Willows and Hoyle 1967, 1969). The circuitry controlling this behavior can be studied in isolated brain preparations in which the swim motor pattern is triggered by electrical stimulation of a body wall nerve (Dorsett et al. 1973). The swim CPG (Fig. 1) is composed of three interneuron types, which have been suggested to be sufficient for generating the swim motor pattern: there are three dorsal swim interneurons (DSIs; http://www.neuronbank.org/Tri0001043), one ventral swim interneuron (VSI-B; http://www.neuronbank.org/Tri0002436), and one cerebral neuron 2 (C2; http://www.neuronbank.org/Tri0002380). Each interneuron has a contralateral counterpart (Getting 1989a). Extrinsic input from sensory pathways is conveyed by the dorsal-ramp interneuron (DRI; http://www.neuronbank.org/Tri0002471), which depolarizes the DSIs (Frost and Katz 1996). The DSIs are serotonergic (Katz et al. 1994; McClellan et al. 1994) and function not only as members of the CPG but also as intrinsic neuromodulators, causing widespread cellular and synaptic effects within the network (Katz and Frost 1995a,b, 1997; Sakurai and Katz 2003; Sakurai et al. 2006).

The *Tritonia* swim CPG was initially thought to be controlled exclusively by extrinsic inputs from sensory pathways. Pioneering work by Getting and colleagues showed that electrical stimulation of a body wall nerve produces a long-lasting depolarization of the DSIs that decays over the course of the swim motor program (Getting and Dekin 1985; Lennard et al. 1980). Getting termed this the "ramp" input, characterized this input using voltage-clamp experiments (Getting and Dekin 1985), and investigated its control over the swim CPG using a detailed computational model of the network (Getting 1983a, 1989b). These simulations indicated that the ramp input should be sufficient to control the initiation, maintenance, and termination of rhythmic bursts of action potentials by neurons in the CPG. Later the DRI was identified as the source of the ramp

✠ Deceased 2 July 2003.

Address for reprint requests and other correspondence: R. J. Calin-Jageman, Department of Psychology, Dominican University, 7900 West Division Street, River Forest, IL 60305 (E-mail: rcalinjageman@dom.edu).

The costs of publication of this article were defrayed in part by the payment of page charges. The article must therefore be hereby marked "*advertisement*" in accordance with 18 U.S.C. Section 1734 solely to indicate this fact.

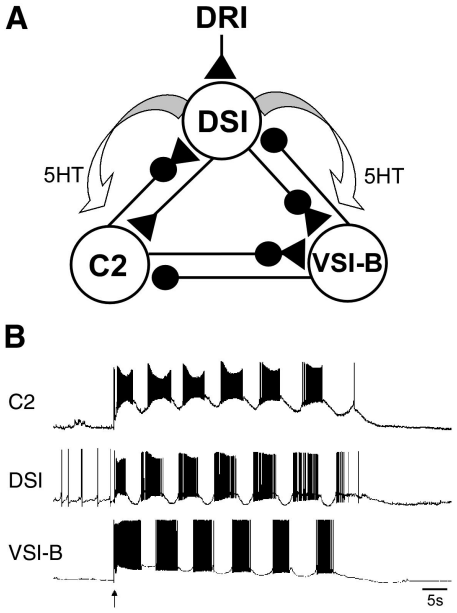

FIG. 1. *A*: the central pattern generator (CPG) core of the *Tritonia* escape swim circuit. This simplified circuit architecture was used for our model of the network. Triangles and circles represent excitatory and inhibitory synaptic connections, respectively. Multiple-component synapses are represented with a triangle and circle. The dorsal swim interneurons (DSIs) release serotonin (5HT), causing widespread cellular and synaptic effects throughout the network. *B*: representative simultaneous electrophysiological recordings made with intracellular electrodes showing a swim motor program evoked by nerve shock (arrow).

input (Frost and Katz 1996). Consistent with Getting's conception of extrinsic control of the CPG, DRI activation is sufficient to trigger the swim motor program, and early termination of DRI activity halts the swim motor program.

Although extrinsic input from DRI exerts strong control over the *Tritonia* CPG, other evidence suggests that intrinsic neuromodulation from the DSIs may also play a crucial role. First, bath application of 5HT causes activation of the CPG in the absence of nerve stimulation (McClellan et al. 1994). Second, bath application of the 5HT-receptor antagonist methysergide blocks swim initiation in the isolated nervous system and in the intact animal. Third, tonic activation of the DSIs themselves can initiate and maintain rhythmic CPG activity (Fickbohm and Katz 2000). Finally, basal excitability of the C2s is too low to support the swim motor program but is elevated dramatically by the neuromodulatory effects of DSI activation (Katz and Frost 1997).

Another potential factor in CPG activation may be the recruitment of additional circuit elements. Specifically, it has now been recognized that C2 makes a recurrent excitatory connection with DRI (Frost and Katz 1996), enabling it to recruit additional excitation into the circuit during the swim motor program. Further polysynaptic pathways within the core CPG may also exist. Thus activation of the swim CPG may actually be quite complex, involving extrinsic input, intrinsic neuromodulation, and additional circuit elements.

The interplay between multiple conditions for activation may have been obscured in Getting's model of the network (Getting 1983a, 1989b). The high-divalent cation solution Getting used does not effectively eliminate polysynaptic interactions (Katz and Frost 1995b). In addition, the model was developed prior to the recognition of intrinsic neuromodulation. It was likely developed from electrophysiological measurements taken after recently evoking the swim motor program, a condition that is now known to produce strong modulation of circuit properties (Frost et al. 1998). Thus Getting's model may have inadvertently incorporated neuromodulatory and polysynaptic effects and thereby underestimated their contribution to activating the network.

To better understand the multiple determinants contributing to activation of the *Tritonia* swim CPG, we developed a new simulation of the network. This model was developed from new physiological data taken from unmodulated, well-rested preparations with monosynaptic connections characterized in a strong high-divalent cation solution effective at blocking polysynaptic pathways. We then explored the contribution of three factors to CPG activation: extrinsic input, the known effects of intrinsic modulation, and the known polysynaptic pathway from C2 to DSI. Surprisingly, none of these factors alone or combined were sufficient to initiate rhythmic bursting in the model circuit. This suggests that activation of the swim motor program is accompanied by additional circuit features that have not yet been documented. To determine, in an unbiased fashion, the types of changes that could enable activation, we conducted a large-scale parameter space analysis, systematically shifting the properties of the rested, unmodulated network toward Getting's original model of the CPG. Our analysis suggests that initiation of the swim motor program involves substantial reconfiguration at multiple sites in the network, indicating distributed control over the production of rhythmic activity via modulatory actions and/or the recruitment of additional circuit elements.

Portions of this work have been reported in abstract form (Calin-Jageman et al. 2006b) and as part of a book chapter (Frost et al. 1997).

METHODS

Physiology

Specimens of *T. diomedea* were obtained from the coastal waters of Washington State and British Columbia. Once in the laboratory, animals were maintained either in running sea-water systems at Friday Harbor Laboratories (11–13°C) or in an artificial seawater system in Houston, TX (11°C). For each experiment, the brain, consisting of the cerebral, pleural, and pedal ganglia, was removed from the animal and immediately placed in a 1-ml recording chamber where it was superfused with normal saline at 2–3°C. The composition of the normal saline was (in mM) 420 NaCl, 10 KCl, 10 $CaCl_2$, 50 $MgCl_2$, 10 HEPES, (pH 7.6), and 11 D-glucose.

To facilitate intracellular recording, the ganglionic connective tissue sheath was usually removed, although occasionally recordings were made with the sheath intact by tapping electrodes directly through the sheath into the visually identifiable somata below. For recordings from VSI-B, half of the brain was rotated 180° around its central commissure, such that the dorsal surface was uppermost on one half and the ventral surface uppermost on the contralateral side. This was done to allow simultaneous recording from soma of VSI-B, which is on the ventral side of the pleural ganglion (Getting 1983b), and C2 and DSI, which are on the dorsal surface of the cerebral ganglion (Getting et al. 1980). To allow the swim motor pattern to be evoked, the left and/or right pedal nerve 3 (PdN3) were sucked up into electrodes made from polyethylene tubing (Intramedic, PE-100) drawn out to a fine tip diameter over a flame.

After the dissection and placement of the suction electrodes, preparations were warmed to 10°C and remained at this temperature for the intracellular electrode impalements and the remainder of the experiment. Intracellular recordings were made using single-barreled glass microelectrodes (10–20 MΩ) filled with either 3 M KCl or 4 M K-acetate. A single electrode was used to pass current and to record voltage except for recordings from VSI-B, in which two independent electrodes were used (1 current passing, 1 recording) to ensure accurate characterization of the voltage dependence of I_A (see following text). Experimental measurements were performed in either normal saline or saline containing a high concentration of divalent cations in which the concentrations of Ca^{2+} and Mg^{2+} were increased 2.5 times relative to normal [composition (in mM): 285 NaCl, 10 KCl, 25 $CaCl_2$, 125 $MgCl_2$, 10 HEPES, (pH 7.6), and 11 D-glucose] to permit the measurement of monosynaptic potentials by raising spike thresholds and blocking polysynaptic contributions (Katz and Frost 1995b). This high-divalent cation solution uses a higher concentration of divalent cations than the one used by Getting (1983a, 1989b) and more effectively eliminates polysynaptic pathways (Katz and Frost 1995b). All neurons were identified on the basis of soma location and coloration, synaptic interactions, and activity pattern during the swim motor program (Getting 1983b). All measurements were made from neurons in rested preparations that were allowed to sit unstimulated for ≥3 h after the end of the dissection, during which time spontaneous activity recorded in PdN3 subsided to a constant minimal level.

Data were stored on magnetic tape using a Vetter 3000 PCM recording adapter (Vetter, Rebersburg, PA). Curve fitting was performed using Sigma Plot software (Systat, San Jose, CA).

Cellular properties

To construct a representative model of each neuron class, several exemplars of each cell type were characterized, each in a different preparation (7 C2s, 5 DSIs, and 3 VSI-Bs). For each exemplar, the resting potential (V_r), input resistance (R_{input}), input capacitance (C), and steady-state action potential threshold (θ_{ss}) were measured under current clamp. Capacitance was determined by dividing the time constant of the input resistance charging curve by input resistance. The tonically active DSIs were silenced by injecting them with hyperpolarizing current to obtain θ_{ss}. Representative values were determined by averaging across the exemplars in each neuron class. Of the three VSI-Bs characterized, values were chosen from the single exemplar with the deepest resting membrane potential. This was done to ensure a good reproduction of I_A, which is strongly voltage-dependent.

Frequency-current (*F-I*) relationships were measured by injecting a range of depolarizing pulses. C2 received 5-s pulses ≤3 nA; VSI-B received 5-s pulses ≤4 nA; DSI received 5-s pulses ≤3 nA and 300-ms pulses from there ≤6 nA (for these shorter, high-amplitude pulses, only initial firing frequency was used). The first and last interspike intervals of each exemplar in a class were plotted against current applied, and a two-component negative exponential curve was fit to each data set (Fig. 2). The resulting functions were used as "typical" initial-firing-interval and final-firing-interval curves for each neuron class. Inverting these functions provided typical initial-frequency and final-frequency curves (Fig. 3).

The VSI-B is notable for a voltage-dependent transient potassium current termed A-current (I_A) that slows the onset of VSI-B's firing response to injected current pulses (Getting 1983b). To characterize this cell, additional measures of its cellular properties were collected (Fig. 4). Specifically, we measured the relationship between current amplitude and delay in onset of VSI-B activity, the voltage dependence of I_A inactivation, and the rate of de-inactivation. These measures provided additional data to constrain our reconstruction of VSI-B.

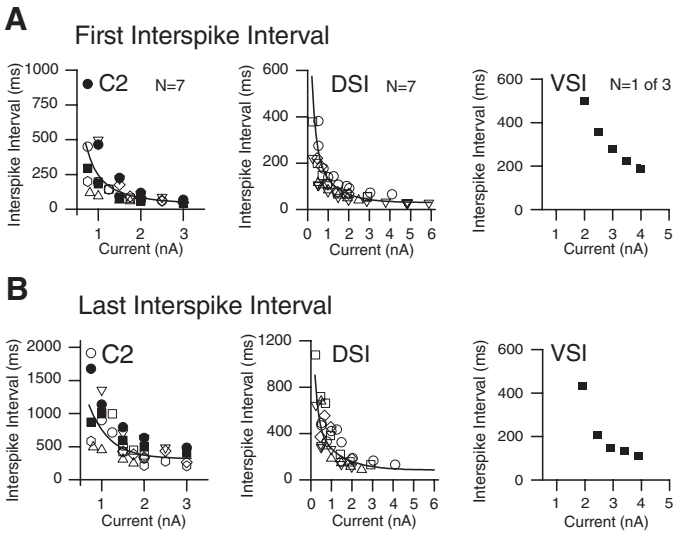

FIG. 2. Characterization of the repetitive firing properties of each of the neurons in the CPG core [DSI, cerebral neuron 2 (C2), and ventral swim interneuron B (VSI)]. Neurons were injected with a series of constant depolarizing 5-s current pulses, and their firing responses were recorded. Each neuron contributing to each data set is represented by a different symbol, and the total number of neurons in each data set is indicated. For VSI-B, a single exemplar with the deepest resting potential was chosen from 3 experiments. This was done to help ensure proper modeling of I_A, which is highly voltage-dependent. *A*: plots of 1st interspike interval versus current. *B*: plots of last interspike interval vs. current. The curve fits from these plots, which represent the typical response profile for each neuron type, were used as templates for constructing the model neurons (Fig. 3).

Model cells

Neurons were simulated using a hybrid integrate-and-fire scheme (Getting 1983a, 1989b) that allows precise reconstruction of complex cellular and synaptic properties with a minimum of free parameters. Complete details on this modeling scheme are contained in Lieb and Frost (1997) and are summarized in the APPENDIX. In this scheme, each model cell is represented as a single isopotential compartment. Although this abstracts significant morphological complexity, comparisons of simultaneous axonal and somatic recordings indicate that it is a reasonably accurate approach for these cell types (Getting 1983a). Moreover, this approach provides model cells with highly accurate current-frequency relationships, indicating accurate replication of firing properties (Lieb and Frost 1997).

In general, a three-step procedure was used to model each cell type. First, the measured mean values of V_r, R_{input}, and C were entered, producing a model cell with passive properties matching those measured in the soma of the real cell. Second, a threshold function and a single spike undershoot-conductance were added, introducing another measured parameter (θ_{ss}) and five free parameters (threshold function: θ_r and θ_τ; undershoot conductance: W, τ_{open}, and τ_{close}). The five free parameters were adjusted to reproduce the initial-frequency curve derived from current injections. For some cell types (e.g., DSI), the firing rate at the highest ranges of the curve could not be fit accurately. In these cases, a voltage-dependent shunt conductance was added, introducing a fixed parameter ($E_{rev} = V_r$), and seven free parameters (G, τ_m, B_m, C_m, τ_h, B_h, C_h). The weight and activation parameters were adjusted to achieve a final match with the initial-frequency curve. The inactivation parameters were set to prevent inactivation throughout the voltage range of the cell. The completion of this step yielded a model neuron with an accurate relationship between current and initial-frequency, but no spike-frequency adaptation. In the final step, one to two additional slow spike undershoot conductances were added and the three to six free parameters adjusted to match both the

final-frequency curve and the rate of adaptation within each firing train.

The VSI-B neuron was modeled with a more complex protocol to ensure faithful reproduction of the effects of its voltage-dependent transient potassium current, I_A. As with the other neuron types, the first step was to set V_r, R_{input}, C, and θ_{ss} from experimental measurements. A voltage-dependent conductance was then introduced to simulate the effects of I_A on VSI-B activity. The free parameters for

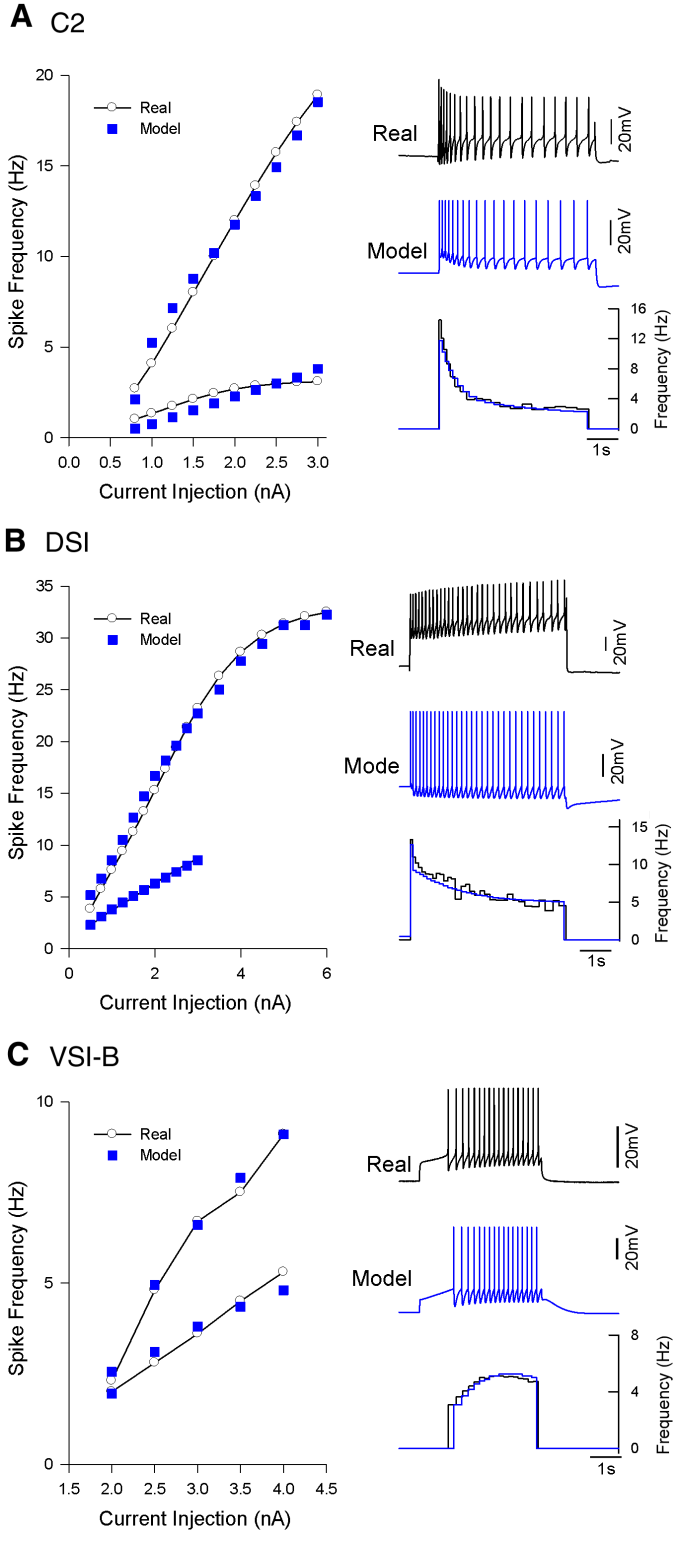

FIG. 3. Comparison of real and model cells. *A*: C2 neuron. *Left*: the instantaneous frequency-current plot for the real (lines with circles) and model (blue squares) C2 neuron during constant current injections of varying amplitude. The *top data set* is the initial firing rate; the *bottom data set* is the final firing rate. *Right*: representative example of activity in the real (*top*) and model (C2) neuron during a 2-nA current injection. Instantaneous frequency across the injection is compared at *bottom*. The model C2 is shown in the blue trace. *B*: DSI neuron. Same as in *A*, but the representative physiology is to a 3-nA current injection. Beyond 3 nA, DSI was injected with 300-ms pulses and only the 1st instantaneous frequency was plotted. *C*: VSI-B neuron. Similar to *A*; however, VSI-B activity accelerates during the current injection so the final-frequency plot is above the initial-frequency plot in the graph at *left*. The representative physiology trace is in response to a 2.5-nA current injection.

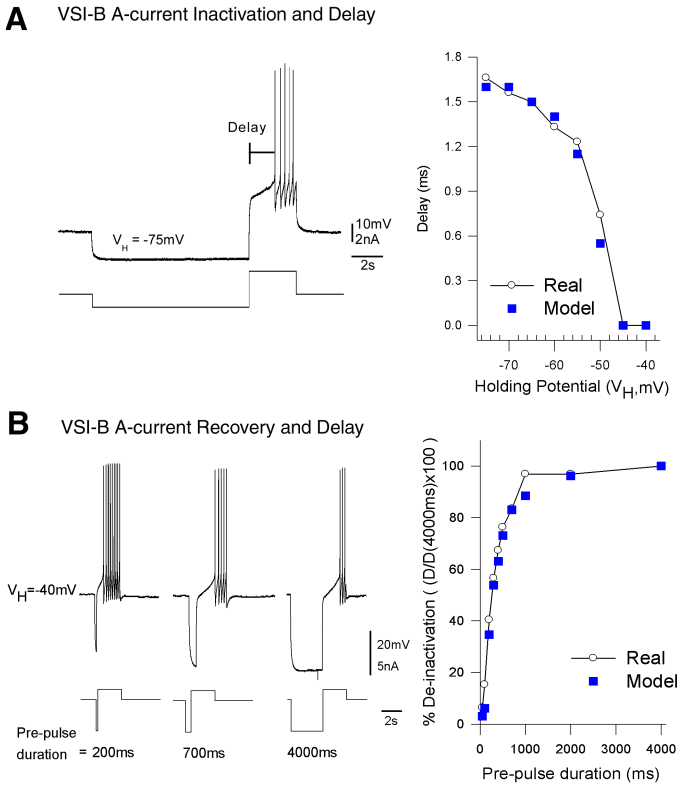

FIG. 4. Comparison of real and model VSI-B on additional protocols used to characterize I_A. Expression of I_A gives VSI-B a distinctive activation pattern, featuring a delay in activation of up to ~2 s and an accelerating spike train. To better model the effects of I_A, we characterized the delay in activation as a function of stimulus amplitude, prior holding potential, and state of activation. *A*: voltage dependence of delay. Voltage dependence of delay was measured with a 2-step current clamp protocol. In the 1st step, a 10-s constant current pulse was applied through 1 electrode to elicit a specific "holding potential," as measured by a 2nd, independent electrode (V_H, range −75 to −40 mV, 5-mV steps). At the end of the 10-s prepulse, the holding current was turned off, and a 2.5-nA depolarizing test pulse was administered to evoke a spike train, from which the delay to the onset of firing was measured. We measured the delay in firing to the test-pulse as a function of the holding potential of the prepulse. A representative example is shown at *left* (real VSI-B). *Right*: a plot of delay as a function of holding potential in both the real (line with circles) and model VSI-B (squares). The asymptote at −45 mV indicates a complete inactivation of I_A at or above this holding potential > −45mV. *B*: de-inactivation. De-inactivation was measured by holding VSI-B to −40 mV (complete inactivation), applying a variable duration conditioning pulse to begin de-inactivating I_A, and then applying a test pulse to evoke VSI-B activity. Representative examples are shown at *left* (real VSI-B). *Right*: a plot of delay as a function of prepulse duration in both the real (line with circles) and model (squares) VSI-B. It can be seen that the model VSI-B accurately captures the distinctive firing properties conveyed by expression of I_A.

this conductance (*W*, E_{rev}, B_m, C_m, τ_m, B_h, C_h, τ_h) were set to match the delay properties of the VSI-B (Fig. 4). The third step was to introduce a pair of spike undershoot conductances, each with free parameters for *W*, τ_{open}, and τ_{close}, to model the repetitive firing properties of VSI-B. Finally, to completely mimic the acceleration of VSI-B firing observed during a sustained activation, an excitatory autosynaptic connection was added with a reversal potential of +10 mV. *W*, τ_{open}, and τ_{close} were adjusted to achieve the degree of acceleration observed in the real cell. Incorporation of I_A into the model VSI-B altered its apparent R_{input}, as the conductance is partially activated at the VSI-B resting potential. The R_{input} originally entered into the model was thus adjusted to produce the same "observable" R_{input} as had been measured empirically.

Postsynaptic potential shape

Synaptic connections between neurons were simulated based on the observed shape of the underlying postsynaptic potential (PSP) and the functional strength of the connection. PSP shape was determined experimentally by making paired intracellular recordings from pre- and postsynaptic neurons and stimulating the presynaptic cell to fire either a single spike for fast PSPs or a brief train of spikes for PSPs with slow components. PSPs were recorded in high-divalent cation solution, so as to record only monosynaptic components. For each connection, a number of examples of recorded PSPs were inspected and a representative example was selected as a template. The model synapse was then developed using one to three underlying conductances, depending on the complexity of the empirical PSP shape. Each conductance introduced one fixed parameter (E_{rev}) and three free parameters (*W*, $\boldsymbol{\tau}_{open}$, and $\boldsymbol{\tau}_{close}$). The free parameters were hand-tuned until a close fit between the model and real PSP shapes was achieved.

Functional connectivity

Functional strength was assessed by driving each presynaptic cell by current injection and recording the change in the firing rate of their postsynaptic target neurons. Several examples of connectivity were collected in different preparations, and the median strength was chosen for modeling. To achieve the same functional strength within the model, the synaptic weights for the connection (*W*) were scaled. All underlying conductances for a synapse were scaled by the same value to preserve the relative amplitudes of the different synaptic components. Thus each model synapse utilizes a realistic PSP shape, but the synaptic weight is set to mimic the effective connection, not the absolute EPSP amplitude. Finally, to represent the entire population of CPG neurons contributing to the swim motor pattern, synapses were scaled by the number of each cell type (DSIs = 6, C2 = 2, VSI-B = 2).

Simulations

Our new model was initially constructed using MARIO, a custom simulation package (Getting 1989b) and later ported into NEURON (Hines and Carnevale 1997, 2001). To compare our model with Getting's prior model, the specifications and parameters described in Getting 1989b were re-implemented in NEURON. The NEURON versions of both models are available on ModelDB (Accession IDs 93325 and 93326, respectively), the on-line repository of computational models (http://senselab.med.yale.edu/senselab/modeldb/) (Hines et al. 2004; Peterson et al. 1996).

Parameter-space analysis

We conducted a large-scale parameter-space analysis of blends between our model of the unmodulated core network and Getting's (1989b) original model of the circuit. Testing a computational model over a wide range of conditions has become an important part of understanding the conditions and tolerances of different network behaviors (Foster et al. 1993; Goldman et al. 2001; Prinz et al. 2003a, b).

This analysis was conducted using NeuronPM (Calin-Jageman and Katz 2006), a system for distributing NEURON simulations using a screen-saver cluster. Clients were 20 PCs with NEURON and NeuronPM installed. Each configuration was run in NEURON for 90 s of simulated time with a 1-ms time step. A triggering input was applied to DSI at 5 s. In each configuration, bursting activity was characterized in each cell type. Burst onset was defined as a group of at least three spikes fired with an instantaneous frequency over 1 Hz. Burst termination was defined as a pause in activity of $\geq$0.5 s (DSI) or 1 s (C2 and VSI-B). A swim cycle was considered a sequence of bursts with onsets ordered from DSI to C2 to VSI-B. Mean swim cycle duration was measured as the sum of intervals from DSI burst onsets divided by the number of cycles. These statistics were calculated during each run of the simulation by NEURON and recorded into a simple text file on each machine running the analysis. NeuronPM uploaded the distributed results files to a central server, where they were parsed and read into a Microsoft Access database (Redmond, WA). To determine the contribution of individual parameters to model behavior, discriminant analyses were conducted in SPSS (SPSS, Chicago, IL). Parameter space maps were constructed using SigmaPlot (Systat Software).

RESULTS

Our goal was to construct an accurate representation of the unmodulated *Tritonia* swim CPG and determine the factors required to produce rhythmic bursting within the network. To ensure an accurate representation of the unmodulated network, all physiological measurements were taken in well-rested preparations (2–3 h after the postdesheathing warm-up to physiological temperature). Furthermore, a high-divalent cation solution was used during measures of synaptic waveforms to ensure the exclusion of any unknown polysynaptic pathways between network elements.

Realistic model of the escape swim CPG

CONSTRUCTION OF THE MODEL. We modeled the three-cell core (DSI, VSI-B, and C2) of the swim circuit thought to be responsible for generating the rhythmic bursting of the swim motor program (Fig. 1). First, the resting properties of each cell type were characterized. A summary of these results is presented in Table 1, (*Cell Parameters*). Next, frequency-current (*F-I*) relationships were measured (Fig. 2) and used to construct model neurons that precisely reproduce the firing properties of their biological counterparts over a wide range of injected currents (Fig. 3). This included the distinctive activation pattern in VSI-B, which exhibited a delay in activation of $\leq$2s and an accelerating spike train during the pulse (Fig. 4). This is presumably due to VSI-B expression of I_A (Getting 1983b).

Synaptic waveforms were modeled by observing the shape of the underlying PSP for each of the six synaptic pairs in the network (Fig. 5). Although monosynaptic, most PSPs showed evidence of multiple components with different time courses. For example, the C2 to DSI connection exhibits both an initial fast excitation and a slower inhibition (Getting 1981; Katz et al. 1994). Despite this complexity, it was possible to develop model synaptic parameters to precisely match the observed PSP waveforms.

TABLE 1. *Complete parameter list*

A. Cell Parameters

Neuron	R_{input}	SE	V_r	SE	C	SE	θ_{ss}	SE	θ_r	θ_τ
C2	23.3	3.49	−48.00	0.46	2.27	4.1	−34	3.7	0	65.0
DSI	38.8	7.39	−47.50	0.39	1.57	2.2	−50	2.2	200	15.0
VSI	14		−56.00		3.2		−38		10	10.0

B. Voltage-Dependent Shunt Conductances

Conductance	G	E_{rev}	B_m	C_m	τ_m	B_h	C_h	τ_h
VSI shunt	1	−70	30	−9	10	54	4	600
DSI shunt	0.08	−47.5	29	−1	10	−100	1.00	100,000

C. Spike Undershoot Conductances

Synapse	W	E_{rev}	τ_{open}	τ_{close}
C2				
Fast	0.12000	−80	10	30
Med	0.02800	−80	10	1,200
Slow	0.00300	−80	4,000	4,000
DSI				
Fast	0.30000	−80	10	85
Slow	0.01200	−80	200	2,800
VSI				
Fast	0.54000	−80	10	100
Slow	0.00460	−80	1,000	2,500

D. Synaptic Conductances

Synapse	W	E_{rev}	τ_{open}	τ_{close}
C2 to DSI				
E_1	0.00029	10	300	300
I_1	0.00063	−80	400	4,000
I_2	0.00018	−80	5,000	14,000
C2 to VSI				
E_1	0.00160	10	500	500
I_1	0.00600	−80	1,300	2,300
I_2	0.00260	−80	7,000	7,000
DSI to C2				
E_1	0.02400	10	10	370
E_2	0.00108	10	2,200	2,200
DSI to DSI				
E_1	0.00058	10	850	1,100
DSI to VSI				
E_1	0.00720	10	300	400
I_1	0.01050	−100	600	700
I_2	0.00120	−100	3,000	3,000
VSI to C2				
I_1	0.00700	−60	300	6,500
VSI to DSI				
I_1	0.05000	−80	34	100
I_2	0.01800	−80	200	750
VSI to VSI				
E_1	0.02800	10	200	500
DRI to DSI (sensory input used to activate network)				
E_1	0.02000	10	25	15,000

Values in *A* are measurements from physiological experiments ± SE except for θ_r, and θ_τ. R_{input} is input resistance, V_r is resting potential, C is membrane capacitance, θ_{ss} is steady-state threshold, θ_τ is the threshold reset, and θ_τ is time constant of decay back to steady-state threshold. For shunt conductances (*B*), G is maximum conductance and E_{rev} is the reversal potential. *B, C,* and θ are the half-maximal steady-state potential, activation slope, and time constant toward steady state, respectively, for both the activation (m) and inactivation (h) terms. Finally for synaptic conductances (*C* and *D*). W is synaptic weight, E_{rev} is the reversal potential, and τ_{open} and τ_{close} are the opening and closing time constants, respectively. Time constants are expressed in milliseconds, membrane potentials in millivolts, capacitance in nanofarads, and resistance in megaohms.

Finally, the strength of each model synaptic connection was set by characterizing the functional connectivity within the network (Fig. 6). In all cases, it was possible to scale the model synapses for an accurate reproduction of the real connectivity within the network. A complete parameter list for the model is presented in Table 1.

COMPARISON TO THE PRIOR MODEL. For comparison, the connectivity in the Getting (1989b) model of this circuit is also depicted in Fig. 6. Although some strong consistencies are evident, it is clear that the Getting model diverges markedly from our empirical measures (e.g., C2 to DSI, C2 to VSI-B, DSI to C2). This suggests that the Getting model does not

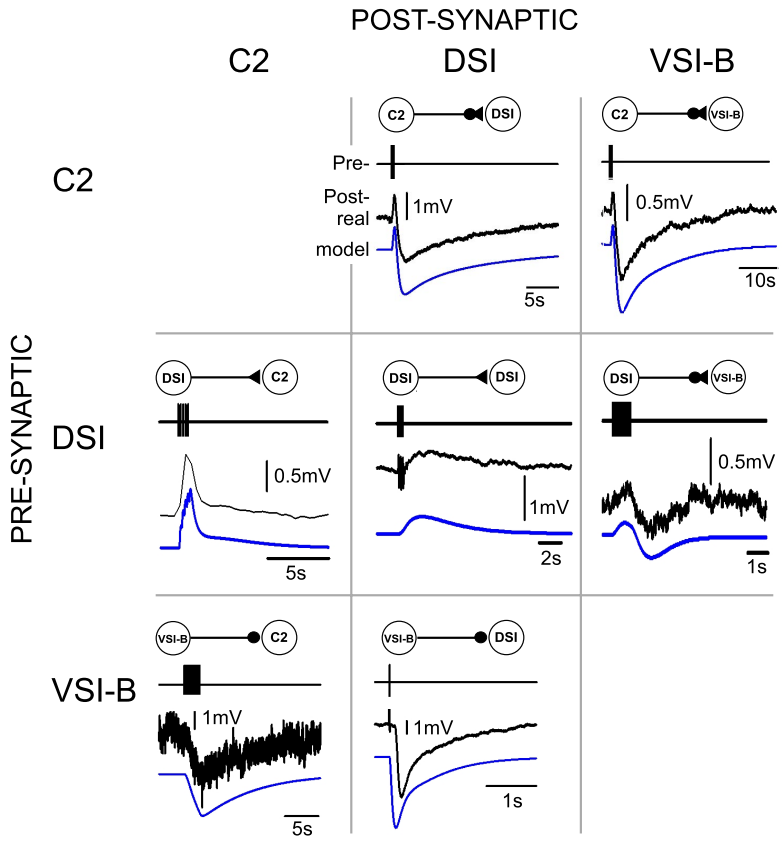

FIG. 5. Comparison of real (black) and model (blue) postsynaptic potential (PSP) waveforms. Physiological measurements were made in a high-divalent cation solution to isolate the monosynaptic PSP. The presynaptic neuron was driven (*top trace*) and the PSP was measured under current clamp. Model synapses were adjusted to precisely replicate the real PSPs recorded.

accurately reflect the rested state of the core network. It seems likely, instead, that Getting (1989b) inadvertently incorporated polysynaptic interactions and/or the effects of intrinsic modulation (see DISCUSSION).

SIMULATED EXTRINSIC INPUT. Experimentally, a swim motor pattern can be evoked by applying an electrical stimulus (5–20 V, 10 Hz, 1 s) to a peripheral nerve. This stimulus evokes a long-lasting "ramp" depolarization in the DSIs (Getting and Dekin 1985; Lennard et al. 1980). The DRIs have been identified as an important source of this ramp input (Frost and Katz 1996). Getting did not directly simulate DRI (which was unknown at the time) but instead delivered input to the model through an excitatory synapse onto DSI. The strength and shape of this input synapse was set to match the amplitude and time course of the ramp depolarization observed in DSI after nerve shock (Getting and Dekin 1985). We adopted the same approach and modeled extrinsic input as an excitatory synapse onto DSI (labeled DRI-DSI synapse, Fig. 1). The synaptic parameters for this input were matched to the input used in Getting's (1989b) model (Fig. 7*A*). Nerve-shock activation was modeled as a 10-Hz, 1-s stimulation of this input synapse.

Known contributions to circuit activation

The completed model represents a careful reconstruction of the unmodulated state of the CPG core of the *Tritonia* swim network. Moreover the output of the completed model CPG captures the resting state of the network accurately—exhibiting tonic DSI firing at ~1 Hz and no C2 or VSI-B activity (Fig. 7*B1*). We next examined how known features of the circuit contribute to the initiation of the swim motor program.

EXTRINSIC INPUT. A key trigger for the swim motor program is the onset of a prolonged ramp input from DRI (Frost and Katz 1996; Getting and Dekin 1985; Lennard et al. 1980). We thus sought to determine if this input alone is sufficient to trigger rhythmic bursting in the model network. As shown in Fig. 7*B1,* extrinsic input (arrow, 1 s, 10 Hz DRI-DSI activation) did not cause a swim motor program in the model. Instead we observed brisk DSI activity, a few C2 spikes, and a net inhibition of VSI-B.

To ensure that this failure was not due to insufficient activation, we systematically increased both the weight (W) and duration (τ_{close}) of the input synapse (DRI-DSI) by >100-fold. Although this produced more DSI and C2 activity, no amount of sensory input was sufficient to elicit VSI-B activity, a necessary component of the three-part rhythm of the swim motor program. Thus extrinsic input alone is not sufficient to switch the resting system into a rhythmically active system.

The lack of activation could be due to measurement error made during construction of the model. To examine this possibility, each parameter in the circuit was varied by ±15% (a total of 268 simulations). Within this range, the model never exhibited rhythmic bursting at rest nor in response to extrinsic input. Thus even substantial measurement error cannot account for the inability of extrinsic input alone to trigger the swim motor program.

For comparison, activation of Getting's model (Getting 1989b) of the swim CPG is illustrated in Fig. 7*B2*. Although not an accurate representation of the unmodulated network, this model responds to extrinsic input with rhythmic bursting that is very similar to a swim motor program. Moreover, the

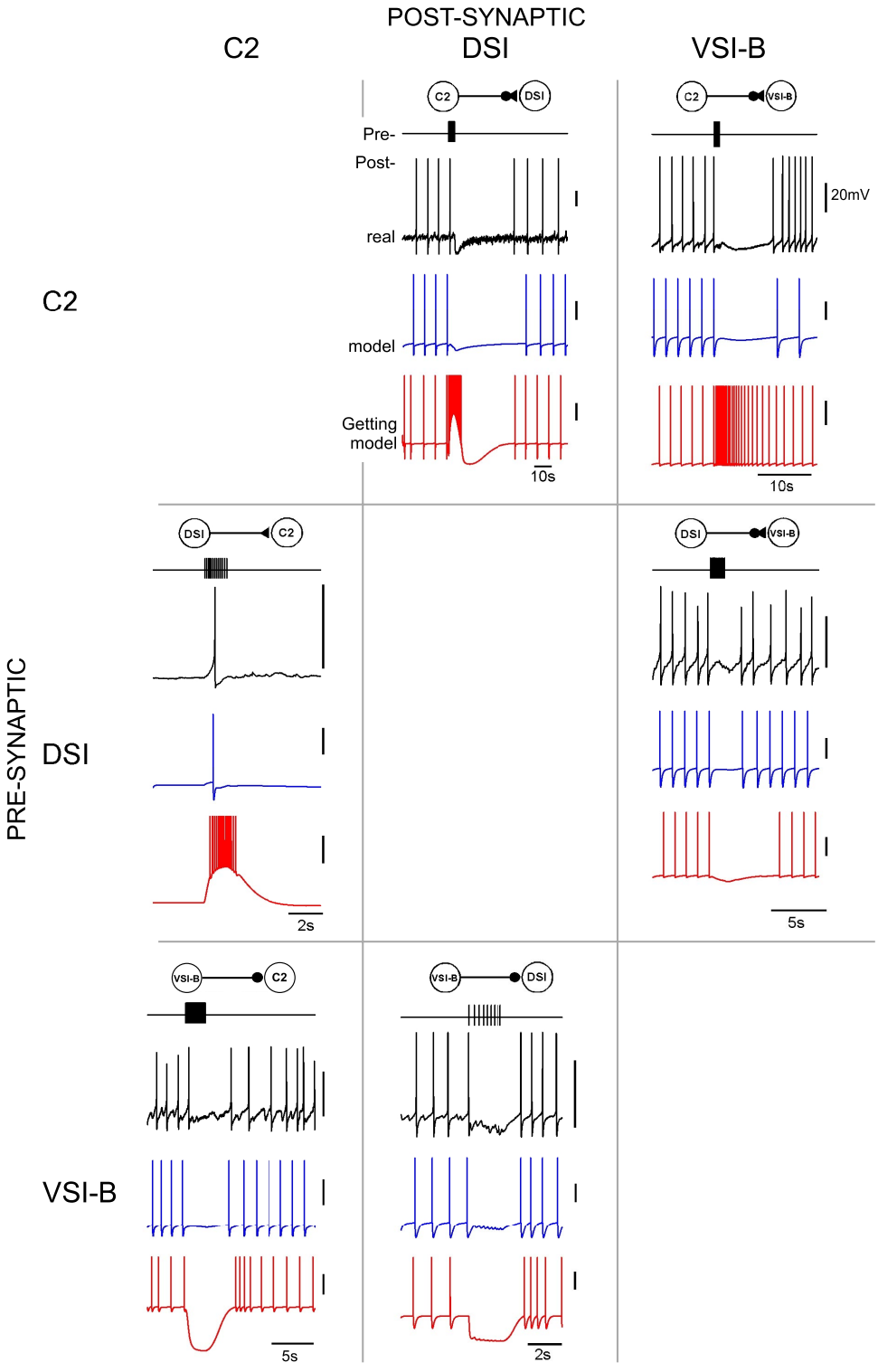

FIG. 6. Comparison of functional connectivity in the real network (black), our new model (blue), and Getting's (1989b) original model of the network (red). For physiological measurements, the presynaptic neuron was driven to fire a train of spikes (*top trace*), and postsynaptic activity was recorded. Model synapses were scaled to have the same functional connection strength as their biological counterpart (the same effect of presynaptic activity on postsynaptic firing). The Getting model shows a marked divergence from the real network at most neuron pairs.

Getting model is not overly sensitive to the level of extrinsic input; it was possible to lower the weight (W) of the input synapse (DRI-DSI) by >40% and still produce a three-cycle swim.

INTRINSIC NEUROMODULATION. The failure of extrinsic input to initiate rhythmic activity suggests the existence of additional requirements for initiating oscillation in the network. One likely candidate is the intrinsic neuromodulation that occurs due to initial activation of the serotonergic DSIs. The known effects of this intrinsic modulation include an increase in C2 excitability via a decrease in spike-frequency adaptation (SFA) (Katz and Frost 1997), an increase in C2 synaptic strength

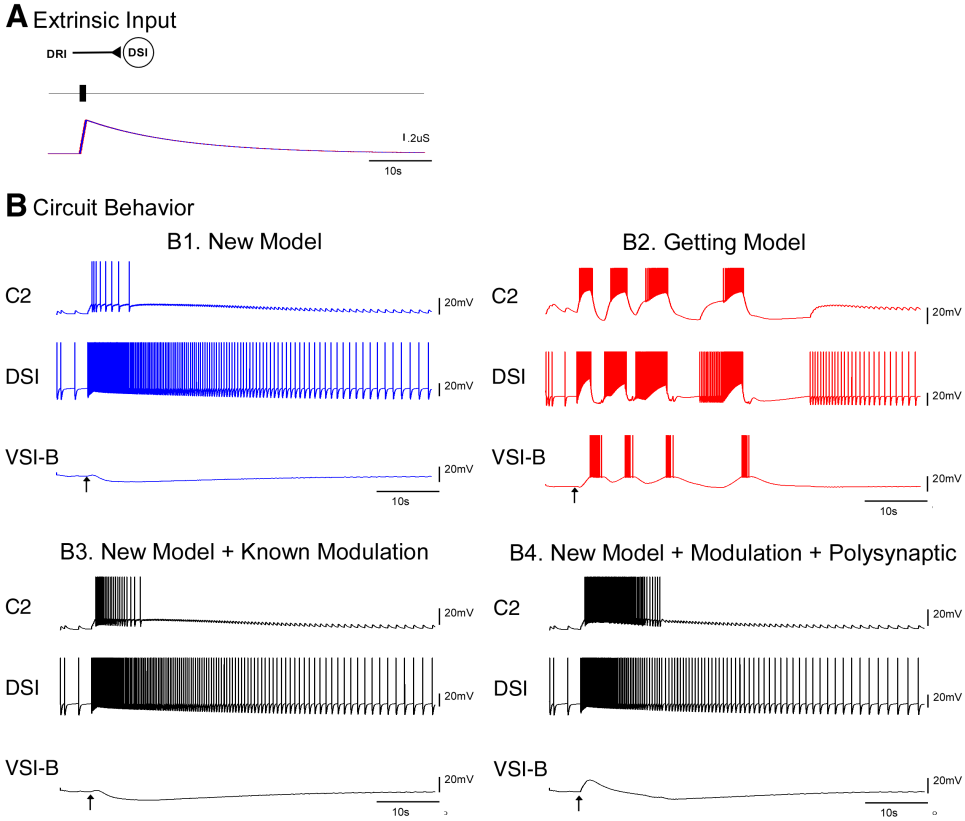

FIG. 7. *A*: extrinsic input to the model. The model was stimulated with a 1-s, 10-Hz train activating the dorsal-ramp interneuron (DRI)-DSI synapse. The *top trace* shows the simulated DRI spikes; the *bottom trace* shows the resulting synaptic conductance onto DSI. Getting developed the parameters for this synapse, reproducing the long-lasting depolarization of DSI elicited by nerve stimulation. We used the same extrinsic input for our new model. *B*: responses of network to extrinsic input delivered to DSI (arrow). *B1*: response of the new data-based model of the unmodulated core CPG (blue). The new model network accurately reflects the cellular and synaptic properties of the unmodulated core CPG network, but it fails to produce rhythmic activity. *B2*: the response of Getting's model (1989b) of the CPG (red). The Getting model produces 3-part rhythmic bursting that is similar to the swim motor program. *B3*: the new model modified to reflect known modulatory actions of DSI. Specifically, C2 spike-frequency adaptation has been reduced by 1/3, all C2 synaptic components have been strengthened by a factor of 3, and VSI-B excitatory synapses have been increased by a factor of 2. These changes are not sufficient to enable rhythmic bursting in the model. *B4*: the new model modified to reflect known modulatory and poly-synaptic influences. C2 recruitment of additional excitation has been modeled by further scaling C2's excitatory synapses up to a factor of 10. Ramp input onto VSI-B has been modeled by adding a DRI to VSI-B synapse activated in tandem with the DRI to DSI synapse (arrow). In addition, all the modulatory effects described in *B3* have been implemented. These changes are not sufficient to enable rhythmic bursting in the model.

(Katz et al. 1995a,b), and a dynamic regulation of VSI-B synaptic strength (Sakurai and Katz 2003; Sakurai et al. 2007).

We next examined if incorporating these modulatory effects into the model would be sufficient to enable rhythmic bursting. First, C2 SFA was decreased by reducing the auto-inhibitory conductance of the model cell until it produced three times as many spikes to 2 nA of current, similar to observations made by Katz and Frost (1997). This did not enable rhythmic bursting at rest or during extrinsic input. We then added an increase in C2 synaptic strength by scaling the weights of each C2 synaptic component by a factor of 3, similar to previous reports (Katz and Frost 1995a,b). Again, this did not enable the model CPG to produce rhythmic bursting. Finally, we strengthened VSI-B excitatory synapses by a factor of 2, similar to the initial heterosynaptic potentiation produced by DSI activation (Sakurai and Katz 2003; Sakurai et al 2007). However, as no VSI-B spikes were generated at rest or during activation, this had no effect on the model.

In case the magnitude of these modulatory effects had been underestimated, we further reduced C2 SFA (medium and long auto-inhibitory conductances were completely removed), scaled all C2 synapses by a factor of 10, and increased VSI-B excitatory synapses by 10. Even these large modifications were insufficient to enable rhythmic bursting. As shown in Fig. 7*B3,* there was almost no impact on the model network at rest or during extrinsic input.

POLYSYNAPTIC PATHWAYS. The inability to initiate rhythmic bursting within our model CPG could also indicate the omission of interposing elements that contribute to the core network. For example, C2 is known to provide a recurrent excitatory connection to DRI via a polysynaptic pathway, which further activates the DSIs (Frost and Katz 1996). Moreover, VSI-B receives some direct excitatory input during the swim motor program (Getting and Dekin 1985). To mimic these polysynaptic interactions, we scaled the excitatory components of C2's synapses onto DSI by a factor of 10 and added an excitatory ramp input to VSI-B (same as the DRI-DSI input). We did this alone and in conjunction with the modulatory changes described in the preceding text (Fig. 7*B4*). In all configurations tested, however, VSI-B remained distant from threshold and no rhythmic bursting occurred.

Exploration of activation conditions

Taken together, these results indicate that the known elements of the swim CPG, including the known neurons, synaptic connections, and intrinsic neuromodulation by DSI, are all insufficient to account for the initiation of the swim motor program in the *Tritonia* swim CPG. This suggests that the activation of the swim motor program is accompanied by additional circuit features that have yet to be documented. These could include neuromodulatory changes in cellular and synaptic properties as well as additional, but as yet unidentified, CPG elements. It could also mean that our estimates of neuromodulatory actions, measured under static control conditions, do not scale well to the dynamic bursting conditions during the production of the swim motor pattern. To determine, in an unbiased way, the circuit features required for rhythmic bursting, we conducted a large-scale parameter space analysis of our new model of the CPG. By systematically varying parameters in the model and cataloguing its output, we could precisely determine the range of network conditions that enable circuit activation.

DIMENSIONS OF EXPLORATION. To guide our parameter-space analysis we used Getting's original model of the circuit (Getting 1989b). Specifically, we compared the functional connectivity of Getting's model to our physiological measurements (Fig. 6). Notable differences in connectivity represent errors in Getting's model that could be due to measurement error, failure to control for modulatory effects, and/or failure to eliminate polysynaptic recruitment. However, Getting's model produces rhythmic bursting similar to the swim motor program, so some of these errors could represent circuit features important for enabling rhythmic bursting. In addition, we planned a broad and extensive parameter-space analysis to ensure a relatively unbiased search for conditions influencing rhythmic bursting.

Discrepancies between Getting's model and the physiological data were identified by comparing functional connectivity, which integrates differences in both synaptic and cellular properties (see METHODS) and thus allowed us to identify a manageable set of parameters most likely to contribute to rhythmic bursting. We found that Getting's model was similar to our physiological measurements of VSI-B to DSI and DSI to VSI-B connectivity, but very different in the other four synaptic pairs (see Fig. 6). For each significant difference, we refit our model's synaptic parameters to replicate the functional connectivity in Getting's model and identified three intermediate settings between these two endpoints (Fig. 8*A*). Overall, this procedure required changes to eight synaptic parameters (Table 2), thereby identifying the parameters most likely to contribute to rhythmic bursting. To determine how these changes would interact with different levels of circuit input, we also varied the strength of extrinsic input (DRI-DSI.E.W) as a ninth parameter.

Applying this new parameter set to our model resulted in a complete change in circuit output—the model now produced rhythmic bursting very similar to the swim motor program (Fig. 8*B*). Note that this configuration produces rhythmic bursting spontaneously unless the DSIs are hyperpolarized. This is the same behavior exhibited in Getting's model (Getting 1989b).

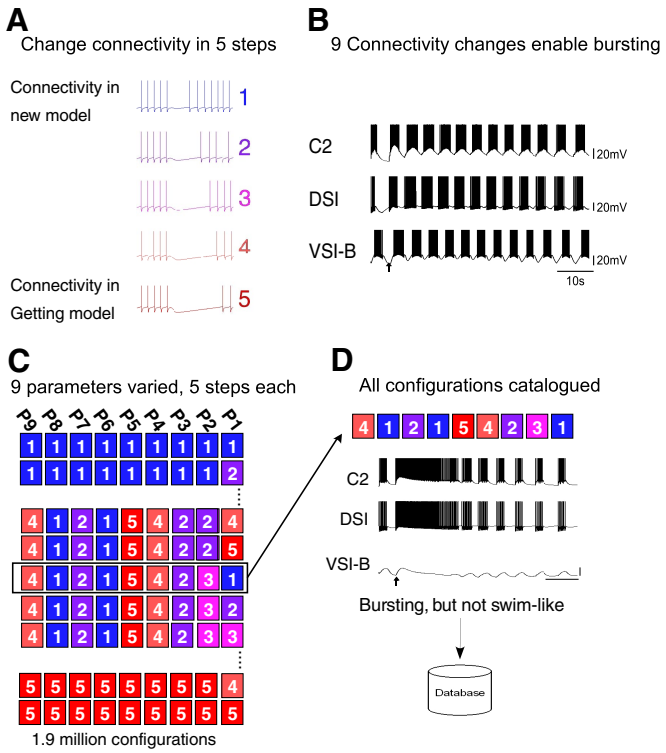

FIG. 8. Construction of a large-scale parameter space analysis of rhythmic bursting. To guide our parameter-space analysis, we used Getting's original model of the circuit (Getting 1989b). *A*: we compared functional connectivity across our new model and Getting's model. Where differences were notable, we refit the synaptic parameters in our model to reproduce connectivity in Getting's model. Shown here, the synaptic changes were made in 5 even increments to gradually shift connectivity in our model toward the Getting model (VSI to C2 synapse is shown). For clarity, each parameter level is color coded with blue representing connectivity in our original model and red representing connectivity similar to the Getting model. *B*: across the entire network, 8 synaptic changes were necessary to match functional connectivity between the models. The level of extrinsic input was also varied as a 9th parameter. Applying this new parameter set to the model enabled rhythmic bursting similar to the swim motor program. *C*: we systematically varied all 9 parameters along their 5 values, simulating 1,953,125 distinct configurations. Shown here are representative configurations based on the matrix of 9 parameters, each taking on 5 levels. Each row is a separate configuration, showing the levels of each parameter. *D*: the output of each configuration was catalogued for analysis. Shown is a single configuration from the parameter-space matrix and the resulting model output when configured in this way.

To explore the performance of our model over a large range of parameter space, we varied each of the nine parameters over five different levels: the value in our model, the value mimicking Getting's model, and three evenly spaced intermediates between these extremes. All 5^9 (1,953,125) intermediate configurations were separately simulated (Fig. 8*C*). For each configuration, the pattern and timing of bursting activity was characterized and catalogued (Fig. 8*D*; see METHODS).

MODEL BEHAVIORS. Rhythmic bursting was rare in the parameter space that we explored (Fig. 9). As in our data-based model of the unmodulated core CPG, 78% of the intermediate configurations exhibited a train of DSI and C2 activity with little or no VSI-B activity (Fig. 9*A*). The other 22% exhibited some level of rhythmic activation (>2 bursts for ≥1 cell type), but this was often restricted to only two cells (Fig. 9*B*). Only 4% of the configurations tested exhibited the three-part bursting typical of the swim motor program (Fig. 9*C*; >2 bursts in

TABLE 2. *Parameters varied, ranges, and discriminant function loadings*

Pre	Post	Synapse	Parameter	Range	D Loading
DSI	C2	E_{1-2}	τ_{close}	×3	0.36*
DSI	C2	E_{1-2}	W	×7.5	0.46*
C2	VSI	E_1	W	×25	0.51*
C2	VSI	I_{1-2}	W	×0	0.51*
C2	DSI	E_1	W	×21	0.23*
C2	DSI	E_1	τ_{close}	×2.5	−0.04
C2	DSI	I_{1-2}	W	×0	−0.03
VSI	C2	I_1	W	×4	0.00
DRI	DSI	E_1	W	×10	−0.15

These 9 parameters were varied from their initial values in the new model (Table 1) to the level required to mimic functional connectivity in Getting's model (range) in 5 even steps. D loading is the factor loading for this parameter in a discriminant analysis examining its influence on producing swimlike bursting. *Strong positive loading.

DSI, VSI-B, and C2). From these, we selected configurations with a regular burst order (DSI, C2, then VSI-B) and a physiologically plausible cycle period (5–11 s). These criteria highlighted a set of 32,524 configurations (1.7% of total) exhibiting rhythmic bursting very similar to the swim motor program (Fig. 9*D*). We considered this group to represent "swimming" configurations and all others to represent "nonswimming" configurations.

The swimming configurations that were identified exhibited considerable variability in several parameter values. This suggested the possibility that swim-like bursting behavior could emerge in multiple, distinct ways from the network. To test this possibility, we used an algorithm to "walk" through the swimming parameter configurations (movement of ±1 parameter level). If swimming configurations were clustered in distinct groups, then some configurations would be isolated from others (impossible to reach via this type of walk). We found, however, that from any given swimming configuration, it was possible to reach all other swimming configurations via this simple walk algorithm. This suggests a lack of distinct subgroups of swimming configurations. Instead, it suggests the presence of a single, continuous area of swimming configurations in the parameter space.

DETERMINANTS OF RHYTHMIC BURSTING. To understand the contribution of each parameter to the production of swim-like bursting, we conducted a discriminant analysis (Johnson and Wichern 1992). Discriminant analysis uses a set of independent variables to produce a function to predict the value of a dichotomous dependent variable. In this case, we entered the nine parameters varied to generate a function classifying each configuration's swim status (swim or no swim). The resulting discriminant function correctly classified 92.9% of the nonswimming and 99.7% of the swimming configurations. The misclassified nonswimmers were primarily three-part bursters that had been excluded due to irregular ordering or cycle frequency.

The discriminant function loading (D Loading) for each parameter is listed in Table 2. These loadings reflect the overall correlation between the parameter and swim status. We found that five parameters had a strong positive impact on swim status (C2-VSIB.E.W, C2-VSIB.I.W, DSI-C2.E.W, DSI-C2.E.τ_{close}, and C2-DSI.E.W) and three had a negligible impact on swim status (VSIB-C2.I.W, C2-DSI.I.W, and C2-DSI.τ_{close}). The strength of extrinsic input had a mild negative impact on swim status (DRI-DSI.E.W). This was due to a tendency of strong extrinsic input to drive tonic activity in the DSIs, eliminating bursting.

To understand the functional implications of this analysis, we first analyzed plots of the univariate effects of each parameter. As shown in Fig. 10, these plots show the likelihood of swim-like bursting across all configurations as a parameter is stepped from its initial to its final value; a nonzero slope

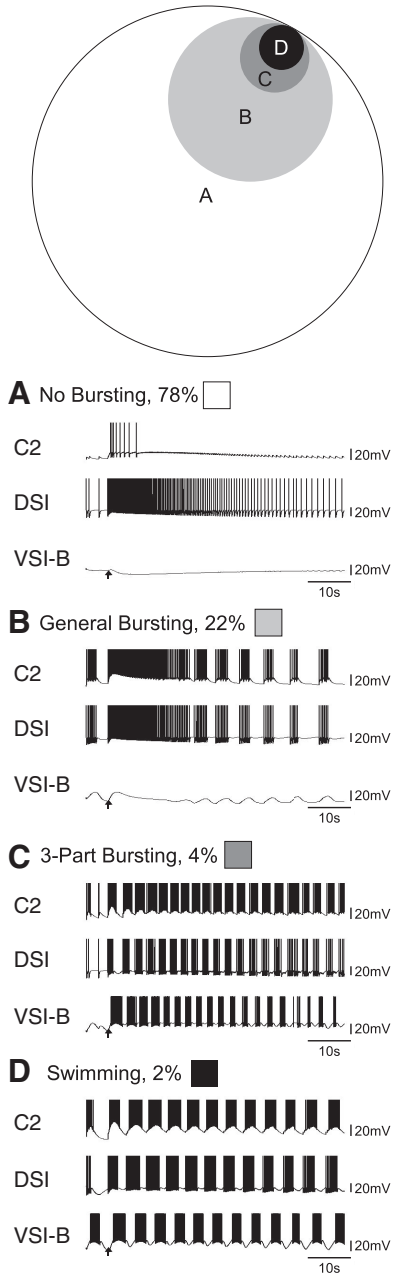

FIG. 9. Venn diagram of the diversity of model behaviors. Each of the 1.9 million configurations was classified as nonbursting (<3 bursts for each neuron), general bursting (>2 bursts for any neuron), or 3-part bursting (>2 bursts for each neuron). "Swimming" configurations were selected from 3-part bursters with realistic burst ordering (DSI, C2, then VSI-B) and cycle period (5–11 s). Examples of each behavioral class are shown at the *bottom* (*A–D*). The relative frequency of each behavioral class is shown at *top*.

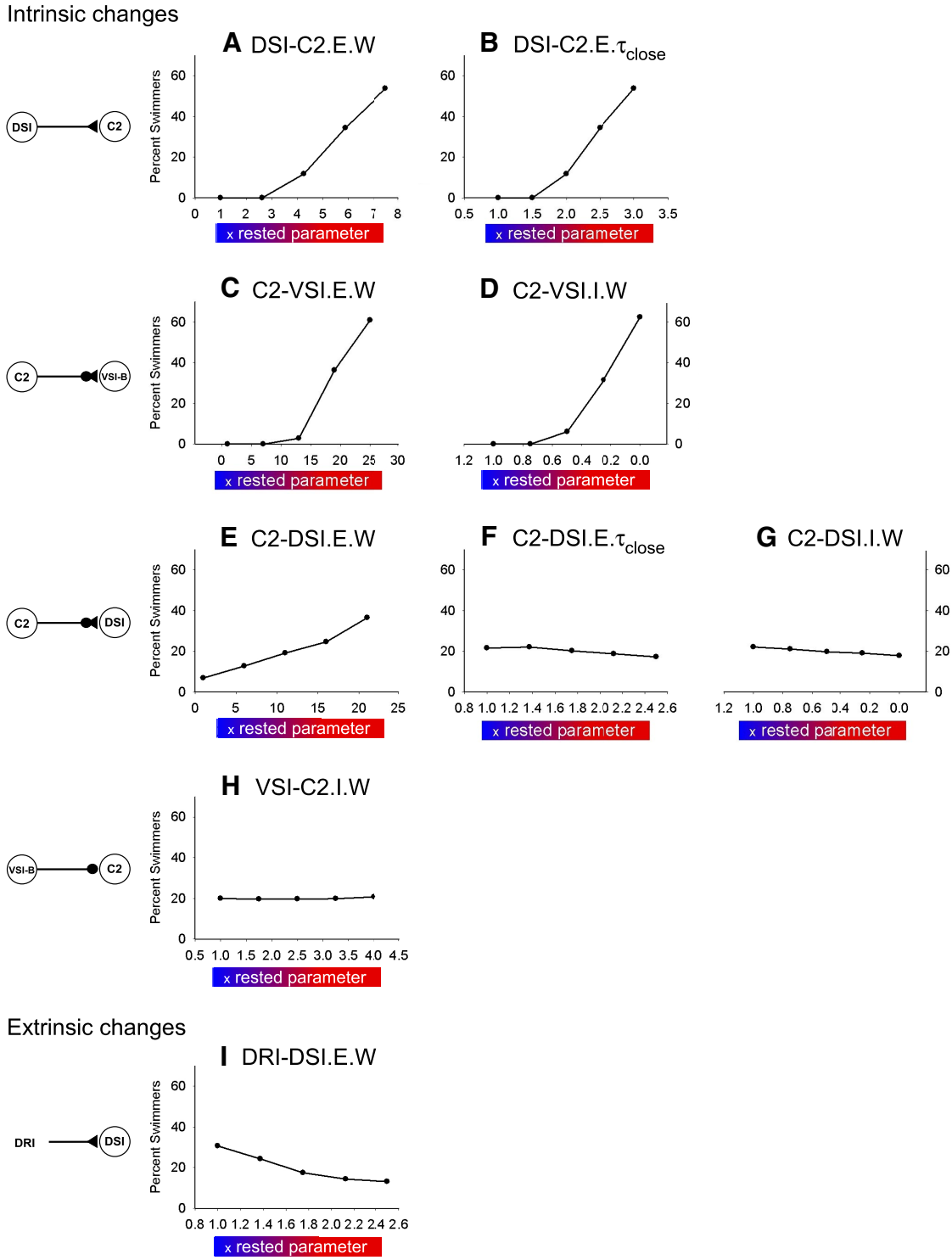

FIG. 10. Univariate effects of parameter changes on model behavior. In the parameter space analysis, 9 synaptic parameters were varied, each taking on 5 different values (5^9 = 1,953,125 simulations). Thus for each level of each parameter, a total of 5^8 (390,625) simulations was conducted. Each panel shows the percentage of these configurations exhibiting swimming (*y* axis) as each parameter was varied from its initial value (*x* axis, expressed as multiples of initial value). This expresses the overall effect of changes in the parameter across diverse network configurations. Positive slopes indicate selection for swimming configurations.

indicates control over swim-like behavior. As predicted by the discriminant analysis, the five parameters with positive loadings show a positive slope in these univariate plots (Fig. 10, *A–E*). Moreover, it can be seen that the top four parameters (Fig. 10, *A–D*) are not only important for swimming but also necessary; swimming never occurs when any one of these parameters is at its initial value. These parameters govern C2 to VSI-B connectivity and DSI to C2 connectivity. Thus these components of the network can gate the production of the swim motor program.

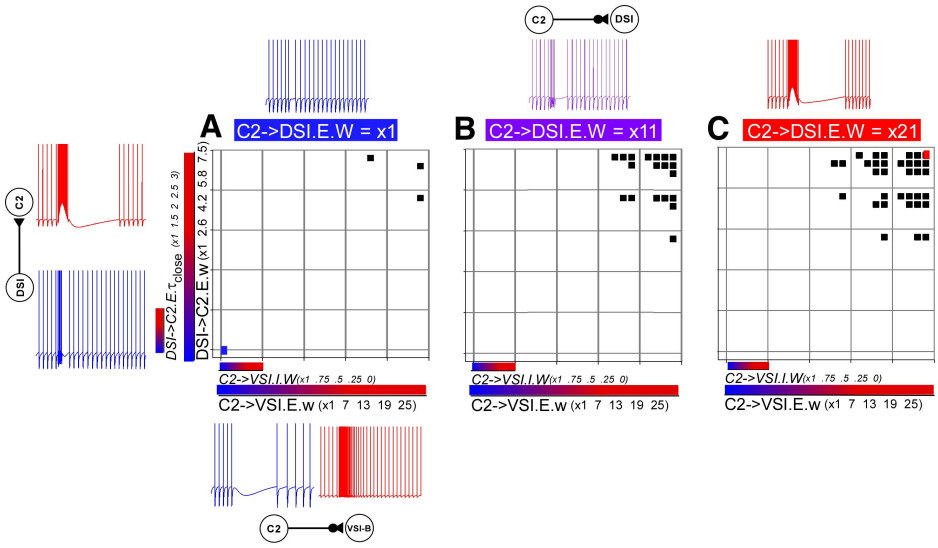

FIG. 11. Parameter-space map showing the organization of swimming configurations by the 5 positive-loading parameters (of 9 explored). To represent this 5-dimensional space, multiple parameters are "stacked" or "embedded" along a single axis, a technique known as dimensional stacking that produces a subgraph of the nested parameter for each level of the parameter it is nested in. Along the *y* axis, DSI to C2 excitatory weight and decay rate are stacked. Changes in these parameters shift the C2 response to DSI activity from weakly excitatory to strongly excitatory (shown next to the axis). On the *x* axis, C2 to VSI-B excitatory and inhibitory weight are stacked. Changes in these parameters shift the VSI-B response to C2 activity from inhibitory to excitatory (illustrated next to the axis). Finally, C2-DSI excitatory weight increases across the 3 panels, changing the DSI response to C2 activity into a very strong excitation. Thus the figure presents a series of parameter-stacks that capture much of the 5-dimensional space defined by these parameters. Swimming configurations are marked in black. The configuration representing the new data-driven model is marked in blue (*bottom left* of *A*); the configuration representing the original Getting model is marked in red (*top right* of *C*). Parameter values are expressed in multiples of their original value (the empirically determined value measured to develop the model).

The fifth parameter with a positive loading governs the strength of the C2 to DSI connection (Fig. 10*E*), which is part of the only recurrent excitatory loop within the network (C2 and DSI). Modification of this connection is important, but not required, as some swimming configurations exist with this parameter at its initial value. To determine the precise role of this parameter in governing the swim, we constructed a parameter-space map (Fig. 11) using dimensional stacking (Taylor et al. 2006). Dimensional stacking reduces a multidimensional space for visualization by "stacking" or nesting multiple dimensions on the same axis, producing a series of sub-graphs showing the nested parameter at each level of another parameter. In this case, we stacked the two parameters influencing DSI to C2 excitability along the *y* axis. Changes in these parameters shift the C2 response to DSI activity from weakly excitatory to strongly excitatory (shown next to the axis). On the *x* axis, C2 to VSI-B excitatory and inhibitory weight are stacked. Changes in these parameters shift the VSI-B response to C2 activity from inhibitory to excitatory (illustrated next to the axis). Each black dot represents a single swimming configuration, localized by its value on these four parameters. Across panels, the strength of C2 to DSI excitability is increased. Thus this figure presents a series of dimensional stacks that highlight how swimming configurations are organized along the five positive-loading parameters. Inspection of the parameter-space map shows that this parameter influenced the range of permissive DSI to C2 and C2 to VSI-B connectivity. With the C2 to DSI connection at its initial level (Fig. 11*A*), swim configurations were only found with the DSI to C2 and C2 to VSI-B parameters at or near their maximal values. As the C2 to DSI connection strengthened, however, swim configurations could be found nearer the initial values of these parameters (Fig. 11, *B* and *C*). In the parameter-space map, this appears as an expanding region of swim states in each panel, representing strengthening of the C2 to DSI connection.

STABILITY OF SWIM CONDITIONS. Swimming configurations were located at the extremes of the parameter space that we analyzed. To determine the range of conditions that support swimming, we extended our analysis around the five parameters with positive loadings, sweeping out an additional five levels on each parameter (10^5 configurations). Again we found a requirement for enhancing DSI to C2 and C2 to VSI-B connectivity with a range-setting role for the recurrent excitatory connection from C2 to DSI (Fig. 12). This larger parameter sweep revealed, however, an extensive pool of configurations that produced swim-like bursting (32%), which extended throughout the highest range of parameter values tested. Again, no isolated groups of swimming configurations were detected, suggesting a single, continuous area within the parameter space. It seems, then, that the production of swim-like bursting can be robust to substantial changes in network properties.

EXTRINSIC INPUT. In characterizing each configuration, extrinsic input was applied to trigger rhythmic bursting. However, the activation of the network did not seem to play a strong role in controlling rhythmic bursting. First, the strength of extrinsic input to the circuit had a negative discriminant loading, indicating that strong input could actually disrupt the swim motor program (Fig. 10*I*). Second we observed that 96% of swimming configurations were still bursting after all extrinsic input has decayed (60 s post stimulation, which is 3 times the time constant of decay for the extrinsic input). This suggests that the swim CPG can operate autonomously, sustaining rhythmic activity without continued input. Consistent with this hypothesis, we noticed that many swim configurations exhibit bursting *prior* to the triggering input. We therefore retested each of the swimming configurations without an input and found that

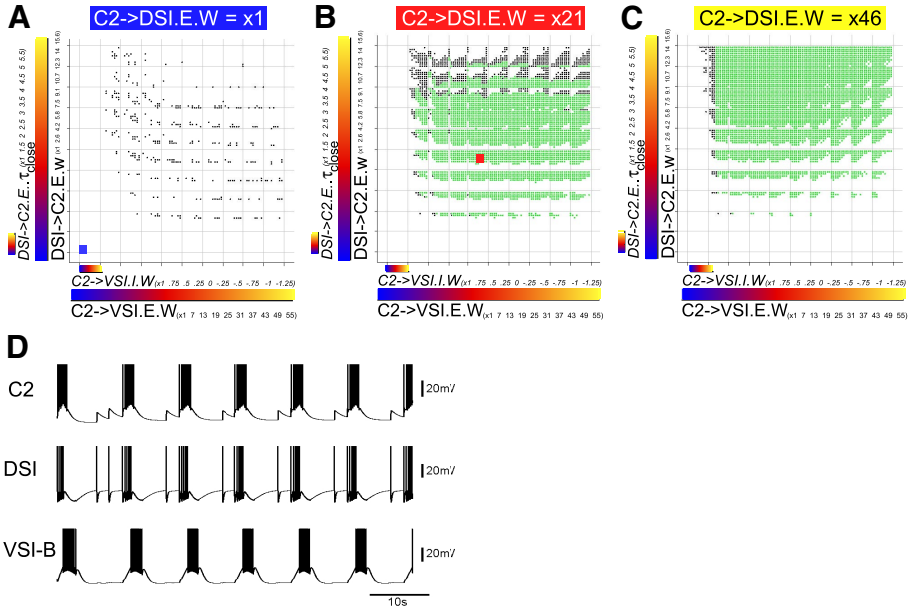

FIG. 12. Partial map of the extended parameter-space showing swimming configurations of the model network. *A–C*: the parameter space analysis was expanded, sweeping out an additional 5 levels for each of the 5 parameters governing swim-like bursting (5^{10} configurations). As in Fig. 7, the 5 parameters governing swim-like bursting were collapsed onto 3 dimensions (dimensional stacking). In each panel, the *y* axis collapses DSI-C2 excitatory weight and decay rate and the *x* axis collapses C2-VSI-B excitatory and inhibitory weight. C2-DSI excitatory weight increases across the 3 panels. Parameter values are expressed in multiples of their original value (the empirically determined value measured to develop the model). Swimming configurations are marked (squares). Swimming configurations exhibiting spontaneous bursting are marked in green, all others are marked in black. *D*: a representative example of a swimming configuration exhibiting spontaneous bursting.

81% exhibited spontaneous rhythmic bursting. Figure 12 presents a representative example of spontaneous bursting (*D*) as well as a partial map of the extended parameter space with spontaneously bursting configurations labeled green (*A–C*).

DISCUSSION

Activation of the *Tritonia* swim CPG is triggered by extrinsic excitatory input but accompanied by intrinsic neuromodulation and the recruitment of additional circuit elements. Here we explored how these dynamic changes contribute to the initiation of rhythmic bursting in the CPG. First, we produced a detailed reconstruction of the core CPG in its rested state. Then we introduced into the model known levels of extrinsic input, intrinsic neuromodulation, and excitatory recruitment. Surprisingly, none of these factors, alone or in concert, were sufficient to initiate rhythmic bursting in the model network. Specifically, elements in the CPG remained too weakly coupled to recruit VSI-B activity and enable rhythmic bursting. This suggests that activation of the swim CPG involves additional features that remain to be discovered. This could include additional excitatory input, modulatory effects, and/or CPG elements, but it could also include some other form of circuit reconfiguration.

Conditions for rhythmic bursting

To delineate the patterns of changes that would unlock the swim motor program, we conducted a parameter-space analysis on our new model of the unmodulated CPG core. This analysis covered an expansive range of circuit configurations and allowed us to precisely determine the circuit conditions that shift the network from quiescent to rhythmically bursting. We found that the transition to rhythmic bursting requires substantial reconfiguration at multiple sites within the network. Specifically, the functional connectivity from DSI to C2 and from C2 to VSI-B must be increased. Without this modification, VSI-B activity cannot be recruited, and the network fails to produce the three-part rhythm that characterizes the swim motor program.

In addition to these requirements, rhythmic bursting is facilitated by increased functional connectivity from C2 to DSI, the only recurrent excitatory connection within the network. The functional connection from C2 to DSI involves feedback recruitment of DRI (Frost and Katz 1996). Increasing connectivity from C2 to DSI amplifies activity within this subnetwork, providing increased activity to recruit VSI-B. This highlights C2 to DSI functional connectivity as a potential control point in the network, which could function to set the threshold for eliciting the swim-motor program (Frost et al. 1998). Computational analyses have previously suggested that the level of recurrent excitation can function as an important determinant for rhythmic activity (Matsugu et al. 1998).

To obtain a manageable set of parameters, our analysis of the network focused on changes in functional connectivity (see METHODS), a technique that captures the combined influence of both cellular and synaptic properties. Thus although we implemented changes in connectivity with altered synaptic parameters, altered connectivity could arise through manifold cellular and synaptic mechanisms.

Mechanisms of activation

The conditions for rhythmic bursting in the model network strongly suggest that extrinsic input is not a sufficient condition for activating the known CPG core. Specifically, the ramp input from DRI can increase DSI and C2 activity but cannot directly increase their ability to recruit VSI-B. Moreover, increased levels of extrinsic input were associated with a decreased probability of rhythmic bursting, as this tended to drive the network toward tonic firing.

Some of the conditions for activation may be met by the recurrent excitatory DSI-C2-DRI-DSI pathway (Frost and Katz 1996; Katz and Frost 1997). The net effect of this interaction would be to couple C2 and DSI more tightly together, which the parameter-space analysis suggests is an important factor in activation. However, incorporating this effect alone could not meet all the conditions for rhythmic bursting in the network, suggesting that additional mechanisms must be involved.

Finally, intrinsic neuromodulation from the DSIs has been proposed to play a role in circuit activation. Consistent with this hypothesis, tonic firing in one DSI can initiate and maintain rhythmic bursting activity in the remaining CPG neurons (Fickbohm and Katz 2000). Moreover, DSI activation enhances C2 excitability (Katz and Frost 1997) and produces an early enhancement of VSI-B synapses (Sakurai and Katz 2003; Sakurai et al. 2006), both of which would serve to meet the requirement for enhanced C2 to VSI-B coupling. However, DSI activation also enhances C2 synaptic efficacy, equally increasing both inhibitory and excitatory components (Katz et al. 1995b). As an inhibitory component dominates the C2 to VSI-B synapse, this effect is likely to *de*couple C2 and VSI-B activity. Moreover, incorporating known modulatory effects into the model did not enable rhythmic bursting.

Taken together, it seems that known levels of extrinsic input, polysynaptic interaction, and intrinsic modulation are all insufficient to account for activation of the swim motor program. In particular, none of these effects were sufficient to enable VSI-B recruitment in the model. This and our parameter-space analysis provide a strong indication that activation also requires factors contributing to VSI-B excitation that remain to be discovered. In the Getting model, VSI-B recruitment occurs because of a strong excitatory monosynaptic connection from C2 to VSI-B. In a strong high-divalent cation solution, however, we observed that this synapse is primarily inhibitory. Thus VSI-B recruitment is likely to occur through an additional circuit element, a modulatory effect that increases VSI-B excitability or excitatory input, or a combination of mechanisms. One possible source of VSI-B excitation is the "ramp" input that occurs during circuit activation (Getting and Dekin 1985). However, adding a slowly decaying ramp input to VSI-B was still insufficient to produce rhythmic bursting in the model. We plan on investigating modulatory effects that could enhance the recruitment of VSI-B activity. In addition, optical recordings may prove useful for searching for the existence of additional circuit elements (Briggman and Kristan 2006; Frost et al. 2007; Morton et al. 1991). As modulatory effects and additional circuit elements are delineated, they can be incorporated into the model circuit to determine if a sufficient set of reconfiguration mechanisms has been identified.

It should be noted that although these results imply that some aspects of the CPG remain to be identified; this does not diminish the role of the known elements. The known core elements are required for the production of the swim motor program (Getting 1983b; Getting and Dekin 1985; Katz et al. 2004), and transient changes in their activity can shift the phase of the swim motor program (Getting 1983b; Getting et al. 1980). Thus it seems that these circuit components will be supplemented, not replaced.

Maintenance and termination of rhythmic bursting

A number of interesting features emerged from the set of rhythmically bursting configurations identified in our extended parameter-space analysis. First, these configurations extended over a large range of network connectivity, spanning order of magnitude changes in several parameters yet producing rhythmic bursting with proper burst ordering and a physiologically plausible cycle frequency. Second, the vast majority of bursting configurations continued oscillating after the decay of extrinsic input. Finally, most of these configurations produced rhythmic bursting spontaneously, in the absence of any input. Thus once configured into a rhythmically bursting state, the model circuit seems to function much like a continuous oscillator: resiliently, continuously, and autonomously. This is consistent with prior observations that the swim-motor program can tolerate large disturbances in the membrane potentials of the neurons in the CPG (Katz et al. 2004).

Dual control of CPG activity

Many episodic CPGs are sensory-gated, switching on in response to fast excitatory inputs from sensory pathways (Jing and Gillette 1995; Rosen et al. 1991; Shaw and Kristan 1997). Other episodic CPGs exhibit intrinsic control mechanisms, requiring changes in network properties to enable rhythmic activity (Dale and Gilday 1996; Staras et al. 2003). Our results suggest that activation of the *Tritonia* swim CPG involves both types of control mechanisms: sensory input as well as a dynamic reconfiguration of network properties. This is similar to activation of the leech swim CPG (Nusbaum and Kristan 1986), which requires extrinsic input from sensory pathways to activate a pair of serotonergic interneurons. Thus the dual requirement of both extrinsic input and intrinsic reconfiguration may represent a common motif in the regulation of CPG activation.

The cooperation of multiple control mechanisms may be important for filtering noisy inputs, thereby providing a relatively high threshold for activating the CPG. In particular, the requirement for intrinsic reconfiguration allows the active and inactive states of the network to be extremely different. This might allow network elements to serve different functions during periods of inactivity. Consistent with this interpretation, elements of the CPG also function in the control of *Tritonia*'s nonrhythmic crawling behavior (Popescu and Frost 2002).

Working model of the Tritonia swim CPG

We have extensively characterized the cellular and synaptic properties of the unmodulated CPG core. Our study suggests that the Getting model (Getting 1983a, 1989b) does not accurately reflect the unmodulated state of this network. Nevertheless, the Getting model exhibits rhythmic bursting that is similar to the swim-motor program. The most likely explanation is that Getting inadvertently incorporated polysynaptic and modulatory effects into the model, thus capturing the network in a bursting state. However, we do not currently have a complete characterization of the modulated circuit, so it is not yet possible to conclusively determine the fidelity of the Getting model. For our analysis, we used the Getting model as a reference point in our parameter-space analysis. Thus even if it reflects a nonphysiological configuration, it has still been a useful sign-post toward understanding the conditions that could enable the swim-motor program.

Another notable aspect of Getting's model is that it produces spontaneous bursting unless the DSIs are hyperpolarized (Getting 1989b). This and the discovery that the DSIs recruit inhibitory input back onto one another (Getting and Dekin 1985) lead to the hypothesis that swim initiation is due in part to C2 activity alleviating this inhibition (Getting 1989b; Getting and Dekin 1985). From our analysis, it seems that tonic

inhibition of the DSIs is not necessary to prevent the swim motor program and that initiation thus involves more complex circuit interactions.

Future work on the *Tritonia* swim CPG simulation will need to include dynamic neuromodulation from the nonmodulated state. It is becoming apparent that static models of neuronal properties may accurately reflect the function of a system in one state, but they do not adequately describe transitions from one state to another such as from resting to rhythmically active.

APPENDIX

Each neuron was modeled as a single iso-potential compartment, with membrane potential (V) varying as

$$\frac{dV}{dt} = -\frac{1}{C}(I_{leak} + \sum I_{syn} + \sum I_{undershoot} + \sum I_{shunt} - \sum I_{stim})$$

Where C is the neuron's measured membrane capacitance, t is time, and the total membrane current is the sum of various leak, synaptic, undershoot, coupling, shunt, and stimulation currents (see following text).

Threshold

Spike threshold was calculated as a function of time from the last spike, t_x

$$\theta(t) = \theta_{ss} + (\theta_r - \theta_{ss})e^{(t_x - t)/\theta_\tau}$$

Where θ_{ss} is the neuron's steady-state threshold (a measured parameter), θ_r is the threshold reset, and θ_τ represents the time constant of decay back to steady state. Every upward crossing of membrane potential past threshold was registered as a spike.

Leak current

Leakage current was calculated as

$$I_{leak} = \frac{V - V_r}{R_{input}}$$

Where V_r is the neuron's measured resting potential and R_{input} is the neuron's measured input resistance.

Chemical synaptic current

Chemical synapses were modeled as an increased conductance, first-order kinetic process

$$\frac{dG_{act}}{dt} = (\text{spike}*1) - \frac{G_{act}}{\tau_{open}}$$

$$\frac{dG_0}{dt} = \frac{G_{act}}{\tau_{open}} - \frac{G_0}{\tau_{close}}$$

$$I_{syn} = W \cdot G_0 \cdot (V - E_{rev}) \cdot A$$

Where G_{act} is the activated but closed conductance state, spike is a switch that equals 1 at the time of a presynaptic spike but 0 otherwise, G_o is the open conductance state, τ_{open} and τ_{close} are the opening and closing time constants, W is synaptic weight, E_{rev} is the reversal potential for synaptic conductance, and A is an empirically derived normalization term, calculated as

$$A = \frac{1}{(4e^{(-3.15/(\tau_{close}/\tau_{open}))}) + 1}$$

Action potential undershoot currents

Action potential undershoots were simulated as auto-synapses with $E_{rev} = -80$ mV.

Voltage-dependent shunt currents

Shunt conductances were calculated as

$$I_{shunt} = G \cdot m \cdot h \cdot (V - E_{rev})$$

where m and h represent activation and inactivation variables for the conductance, respectively. m was calculated as

$$\frac{dm}{dt} = \frac{(m_\infty - m)}{\tau_m}$$

$$m_\infty = \frac{1}{1 + e^{(V_m + B_m)/C_m}}$$

where m_∞ is the calculated steady-state activation, τ_m is time constant of activation, B_m and C_m are constants representing the half-maximal steady-state potential, and activation slope, respectively. h was calculated using the same formulas, but with h_∞, τ_h , B_h, and C_h.

ACKNOWLEDGMENTS

The authors thank C. Morris and J. Medina for contributing to this study. Portions of this work were performed in the Department of Neurobiology and Anatomy, University of Texas Health Sciences Center, Houston, TX

GRANTS

This work was supported by NIH grants to P. S. Katz and W. N. Frost.

REFERENCES

Briggman KL, Kristan WB. Imaging dedicated and multifunction neural circuits generating distinct behaviors. *J Neurosci* 26: 10925–10933, 2006.

Calin-Jageman RJ, Katz PS. A distributed computing tool for generating neural simulation databases. *Neural Computation* 18: 1–5, 2006.

Calin-Jageman RJ, Katz PS, Frost WN. A computational analysis of neuromodulatory control of rhythmic neural activity in the *Tritonia* swim central pattern generator. *Annual Meeting of the Organization for Computational Neuroscience, Edinburgh, Scotland,* 2006.

Dale N, Gilday D. Regulation of rhythmic movements by purinergic neurotransmitters in frog embryos. *Nature* 383: 259–263, 1996.

Dorsett DA, Willows AO, Hoyle G. The neuronal basis of behavior in *Tritonia.* IV. The central origin of a fixed action pattern demonstrated in the isolated brain. *J Neurobiol* 4: 287–300, 1973.

Eisenhart FJ, Cacciatore TW, Kristan WB Jr. A central pattern generator underlies crawling in the medicinal leech. *J Comp Physiol [A]* 186: 631–643, 2000.

Fickbohm DJ, Katz PS. Paradoxical actions of the serotonin precursor 5-hydroxytryptophan on the activity of identified serotonergic neurons in a simple motor circuit. *J Neurosci* 20: 1622–1634, 2000.

Foster WR, Ungar LH, Schwaber JS. Significance of conductances in Hodgkin-Huxley models. *J Neurophysiol* 70: 2502–2518, 1993.

Fredman SM, Jahan-Parwar B. Role of pedal ganglia motor neurons in pedal wave generation in *Aplysia. Brain Res Bull* 5: 179–193, 1980.

Frost WN, Brandon CL, Mongeluzi DL. Sensitization of the *Tritonia* escape swim. *Neurobiol Learn Mem* 69: 126–135, 1998.

Frost WN, Hoppe TA, Wang J, Tian LM. Swim initiation neurons in *Tritonia diomedea. Am Zool* 41: 952–961, 2001.

Frost WN, Katz PS. Single neuron control over a complex motor program. *Proc Natl Acad Sci USA* 93: 422–426, 1996.

Frost WN, Lieb JR Jr, Tunstall MJ, Mensh BD, Katz PS. Integrate-and-fire simulations of two molluscan neural circuits. In: *Neurons, Networks, and*

Motor Behavior, edited by Stein PSG, Selverston AI, Stuart DG, Grillner S. Cambridge, MA: MIT Press, 1997, p. 173–179.

Frost WN, Wang J, Brandon CJ. A stereo-compound hybrid microscope for combined intracellular and optical recording of invertebrate neural network activity. *J Neurosci Methods* 162: 148–154, 2007.

Getting PA. Mechanisms of pattern generation underlying swimming in *Tritonia.* I. Neuronal network formed by monosynaptic connections. *J Neurophysiol* 46: 65–79, 1981.

Getting PA. Mechanisms of pattern generation underlying swimming in *Tritonia.* II. Network reconstruction. *J Neurophysiol* 49: 1017–1035, 1983a.

Getting PA. Mechanisms of pattern generation underlying swimming in *Tritonia.* III. Intrinsic and synaptic mechanisms for delayed excitation. *J Neurophysiol* 49: 1036–1050, 1983b.

Getting PA. A network oscillator underlying swimming in *Tritonia.* In: *Neuronal and Cellular Oscillators,* edited by Jacklet JW. New York: Marcel Dekker, 1989a, p. 215–236.

Getting PA. Reconstruction of small neural networks. In: *Methods in Neural Modeling*, edited by Koch C, Segev I. Cambridge, MA: MIT Press, 1989b, p. 171–196.

Getting PA, Dekin MS. Mechanisms of pattern generation underlying swimming in *Tritonia.* IV. Gating of central pattern generator. *J Neurophysiol* 53: 466–480, 1985.

Getting PA, Lennard PR, Hume RI. Central pattern generator mediating swimming in *Tritonia.* I. Identification and synaptic interactions. *J Neurophysiol* 44:151–64, 1980.

Goldman MS, Golowasch J, Marder E, Abbott LF. Global structure, robustness, and modulation of neuronal models. *J Neurosci* 21: 5229–5238, 2001.

Hines ML, Carnevale NT. The NEURON simulation environment. *Neural Comput* 9: 1179–1209, 1997.

Hines ML, Carnevale NT. NEURON: a tool for neuroscientists. *Neuroscientist* 7: 123–135, 2001.

Hines ML, Morse T, Migliore M, Carnevale NT, Shepherd GM. ModelDB: a database to support computational neuroscience. *J Comput Neurosci* 17: 7–11, 2004.

Jing J, Gillette R. Neuronal elements that mediate escape swimming and suppress feeding behavior in the predatory sea slug *Pleurobranchaea*. *J Neurophysiol* 74: 1900–1910, 1995.

Johnson RA, Wichern DW. *Applied Multivariate Statistical Analysis.* Englewood Cliffs, NJ: Prentice Hall, 1992.

Jordan LM. Initiation of locomotion in mammals. *Ann NY Acad Sci* 860: 83–93, 1998.

Katz PS, Frost WN. Intrinsic neuromodulation in the *Tritonia* swim CPG: serotonin mediates both neuromodulation and neurotransmission by the dorsal swim interneurons. *J Neurophysiol* 74: 2281–2294, 1995a.

Katz PS, Frost WN. Intrinsic neuromodulation in the *Tritonia* swim CPG: the serotonergic dorsal swim interneurons act presynaptically to enhance transmitter release from interneuron C2. *J Neurosci* 15: 6035–6045, 1995b.

Katz PS, Frost WN. Removal of spike frequency adaptation via neuromodulation intrinsic to the *Tritonia* escape swim central pattern generator. *J Neurosci* 17: 7703–7713, 1997.

Katz PS, Getting PA, Frost WN. Dynamic neuromodulation of synaptic strength intrinsic to a central pattern generator circuit. *Nature* 367: 729–731, 1994.

Katz PS, Sakurai A, Clemens S, Davis D. Cycle period of a network oscillator is independent of membrane potential and spiking activity in individual central pattern generator neurons. *J Neurophysiol* 92: 1904–1917, 2004.

Lennard PR, Getting PA, Hume RI. Central pattern generator mediating swimming in *Tritonia.* II. Initiation, maintenance, and termination. *J Neurophysiol* 44: 165–173, 1980.

Lieb JR Jr, Frost WN. Realistic simulation of the *Aplysia* siphon-withdrawal reflex circuit: roles of circuit elements in producing motor output. *J Neurophysiol* 77: 1249–1268, 1997.

Lytonn WW. Neural query system: data mining from within the NEURON simulator. *Neuroinformatics* 4: 163–76, 2006.

Matsugu M, Duffin J, Poon C. Entrainment, instability, quasi-periodicity, and chaos in a compound neural oscillator. *J Comp Neurosci* 5: 35–51, 1998.

McClellan AD, Brown GD, Getting PA. Modulation of swimming in *Tritonia*: excitatory and inhibitory effects of serotonin. *J Comp Physiol [A]* 174: 257–266, 1994.

Morton DW, Chiel HJ, Cohen L, Wu JY. Optical methods can be utilized to map the location and activity of putative motor neurons and interneurons during rhythmic patterns of activity in the buccal ganglion of *Aplysia. Brain Res* 564: 45–55, 1991.

Nagy F, Cardi P, Cournil I. A rhythmic modulatory gating system in the stomatogastric nervous system of *Homarus gammarus.* I. Pyloric-related neurons in the commissural ganglia. *J Neurophysiol* 71: 2477–2489, 1994.

Nusbaum MP, Kristan WB Jr. Swim initiation in the leech by serotonin-containing interneurones, cells 21 and 61. *J Exp Biol* 122: 277–302, 1986.

Peterson BE, Healy MD, Nadkarni PM, Miller PL, Shepherd GM. ModelDB: an environment for running and storing computational models and their results applied to neuroscience. *J Am Med Inform Assoc* 3: 389–398, 1996.

Popescu IR, Frost WN. Highly dissimilar behaviors mediated by a multifunctional network in the marine mollusk *Tritonia diomedea*. *J Neurosci* 22: 1985–1993, 2002.

Prinz AA, Billimoria CP, Marder E. Alternative to hand-tuning conductance-based models: construction and analysis of databases of model neurons. *J Neurophysiol* 90: 3998–4015, 2003a.

Prinz AA, Thirumalai V, Marder E. The functional consequences of changes in the strength and duration of synaptic inputs to oscillatory neurons. *J Neurosci* 23: 943–954, 2003b.

Rosen SC, Teyke T, Miller MW, Weiss KR, Kupfermann I. Identification and characterization of cerebral-to-buccal interneurons implicated in the control of motor programs associated with feeding in *Aplysia. J Neurosci* 11: 3630–3655, 1991.

Sakurai A, Calin-Jageman RJ, Katz PS. The potentiation phase of spike timing-dependent neuromodulation by a serotonergic interneuron involves an increase in the fraction of transmitter release. *J Neurophysiol* In press.

Sakurai A, Darghouth NR, Butera RJ, Katz PS. Serotonergic enhancement of a 4-AP-sensitive current mediates the synaptic depression phase of spike timing-dependent neuromodulation. *J Neurosci* 26: 2010–2021, 2007.

Sakurai A, Katz PS. Spike timing-dependent serotonergic neuromodulation of synaptic strength intrinsic to a central pattern generator circuit. *J Neurosci* 23: 10745–10755, 2003.

Shaw BK, Kristan WB. The neuronal basis of the behavioral choice between swimming and shortening in the leech: control is not selectively exercised at higher circuit levels. *J Neurosci* 17: 786–795, 1997.

Shik ML, Severin FV, Orlovskii GN. Control of walking and running by means of electrical stimulation of the mid-brain. *Biofizika* 11: 659–666, 1966.

Staras K, Kemenes I, Benjamin PR, Kemenes G. Loss of self-inhibition is a cellular mechanism for episodic rhythmic behavior. *Curr Biol* 13: 116–124, 2003.

Taylor AL, Hickey TJ, Prinz AA, Marder E. Structure and visualization of high-dimensional conductance spaces. *J Neurophysiol* 96: 891–905, 2006.

Willows AO, Hoyle G. Correlation of behavior with the activity of single identifiable neurons in the brain of *Tritonia.* In: *Neurobiology of Invertebrates*, edited by Salanki J. New York: Plenum, 1967, p. 443–461.

Willows AO, Hoyle G. Neuronal network triggering a fixed action pattern. *Science* 166: 1549–1550, 1969.